Published in final edited form as:
Neuroscience. 2011 February 3; 174: 71–83. doi:10.1016/j.neuroscience.2010.11.025.

Early-onset dysfunction of retrosplenial cortex precedes overt amyloid plaque formation in Tg2576 mice

Guillaume L. Poirier[*,Ψ], **Eman Amin**[*], **Mark A. Good**[*], and **John P. Aggleton**[*]

[*]School of Psychology, Cardiff University, 70 Park Place, Cardiff, Wales, United Kingdom, CF10 3AT

Abstract

A mouse model of amyloid pathology was used to first examine using a cross-sectional designchanges in retrosplenial cortex activity in transgenic mice aged 5, 11, 17, and 23 months. Attention focused on: 1) overt amyloid labeled with β-amyloid$_{(1-42)}$ and Congo Red staining, 2) metabolic function assessed by the enzyme, cytochrome oxidase, and 3) neuronal activity as assessed indirectly by the immediate-early gene, c-Fos. Changes in cytochrome oxidase and c-Fos activity were observed in the retrosplenial cortex in Tg2576 mice as early as 5 months of age, long before evidence of plaque formation. Subsequent analyses concentrating on this early dysfunction revealed at 5-months pervasive, amyloid precursor protein (APP)-derived peptide accumulation in the retrosplenial cortex and selective afferents (anterior thalamus, hippocampus), which was associated with the observed c-Fos hyporeactivity. These findings indicate that retrosplenial cortex dysfunction occurs during early stages of amyloid production in Tg2576 mice and may contribute to cognitive dysfunction.

Keywords

Alzheimer's disease; posterior cingulate cortex; diaschisis; disconnection; connectivity; energy metabolism

Classical theories of the progression of Alzheimer's disease have drawn attention to the development of pathology in transentorhinal/hippocampal regions during the early stages (Braak and Braak, 1991b; van Hoesen et al., 1991). This view of disease progression has been reinforced by the development of episodic memory deficits during the early stages. There is, however, growing evidence that, in addition to medial temporal lobe structures, the retrosplenial cortex (posterior cingulate region areas 29 and 30) is both vital for episodic memory (Iaria et al., 2007; Maguire, 2001; Vann et al., 2009) and shows evidence of functional abnormalities during the early stages of Alzheimer's disease.

The posterior cingulate region is typically one of the first areas to show metabolic hypoactivity in Alzheimer's disease (Minoshima et al., 1997; Nestor et al., 2003b), with studies of amnestic Mild Cognitive Impairment patients suggesting that the earliest

[Ψ]**Corresponding author**: Guillaume L. Poirier, presently at the Brain Mind Institute, École Polytechnique Fédérale de Lausanne, Switzerland. guillaume.poirier@epfl.ch Tel.: +41 (0)21 693 16 73 Fax: +41 (0)21 693 16 50.

Europe PMC Funders Author Manuscripts

hypoactivity may arise in the retrosplenial cortex (Nestor et al., 2003b). The retrosplenial cortex not only has dense reciprocal connections with the hippocampal formation, but is also interconnected with the anterior thalamic nuclei (van Groen et al., 1993; Vogt et al., 1987; Wyss and van Groen, 1992). The latter nuclei are closely linked to diencephalic amnesia (Aggleton, 2008) and to early pathology in Alzheimer's disease (Braak and Braak, 1993; Thal et al., 2002). Thus, retrosplenial changes in early Alzheimer's disease (Fox et al., 2001; Pengas et al., 2010) may follow from amyloid pathology (Buckner et al., 2005) *and* changes in its afferents (Aggleton, 2008; Fennema-Notestine et al., 2009). Consequently, the retrosplenial cortex appears both directly and indirectly linked with the genesis of cognitive abnormalities in Alzheimer's disease.

The present study used a mouse model of amyloid pathology, Tg2576 APP(swe) mice (Hsiao et al., 1996), to examine the relationship of retrosplenial cortex dysfunction with β-amyloid deposition and the widespread appearance of amyloid plaques, first seen in temporal regions in substantial numbers from 12 months in the brains of this mouse model (Kawarabayashi et al., 2001). Retrosplenial cellular function was evaluated by examining the protein product of the immediate-early gene (IEG) c-*fos*. This IEG is a neural activity-dependent transcription factor (Greenberg et al., 1986) involved in neuroplasticity (Fleischmann et al., 2003; Kasahara et al., 2001; Morgan and Curran, 1991; Nikolaev et al., 1991; Sheng and Greenberg, 1990), and c-Fos hypoactivity in the retrosplenial cortex is associated with pervasive cellular dysfunction (Poirier et al., 2008) and plasticity deficits (Garden et al., 2009). Cellular function was also evaluated using a marker of energy metabolism, cytochrome oxidase (Wong-Riley, 1989), deficient in the posterior cingulate region in Alzheimer's disease (Liang et al., 2008a; Liang et al., 2008b; Valla et al., 2001). Finally, since APP and its metabolites may yield disturbances prior to amyloid plaque formation (Hardy and Selkoe, 2002; Walsh and Selkoe, 2004), we hypothesized that at the earliest stages (5 months old) retrosplenial cortex function would be associated with their appearance locally and in sites providing some of its major inputs (anterior thalamus, hippocampal formation, entorhinal cortex).

Methods

Subjects

Heterozygous male mice expressing the "Swedish" double mutation of the amyloid precursor protein (HuAPP695SWE) with a hamster prion protein promoter; Tg2576 and wild type (WT) littermate control mice in a hybrid background of C57BL/6 × SJL bred and maintained in-house (Chapman et al., 1999; Hsiao et al., 1996) were used in the present study.

Transgenic male mice were compared with male littermate WT controls to ensure that age and background strains were as comparable as possible. Mice at four ages (5, 11, 17, and 23 months) were examined (respectively, 5 months, Tg2576 n = 9, WT n = 9; 11 months, Tg2576 n = 6, WT n = 9; 17 months, Tg2576 n = 8, WT n = 9; 23 months, Tg2576 n = 5, WT n = 4). All animals were housed individually during the course of the experiments. Details of mouse breeding, genotyping, and maintenance of the colony were matched to those described previously (Hale and Good, 2005). The age at the earliest time point was

selected because it is believed to precede the appearance of plaques (10-12 months) in the temporal regions of Tg2576 mice (Hsiao et al., 1996; Kawarabayashi et al., 2001).

Behavioral activity

In order to test for functional differences in retrosplenial cortex activity in the Tg2576 mice, cellular activity in this region was stimulated by exposing the mice to a novel environment. The mice were placed individually in activity test cages (Coulbourn Instruments, Bilaney, Kent, UK) housed in sound attenuating boxes for 10 mins in a novel room, 90 mins prior to perfusion. The activity cages measured 15 × 12 × 14 cm, and were fitted with a ceiling-mounted infrared activity monitor. Locomotor activity was recorded in case that there might be motor differences between the wildtype and transgenic mice that could confound cellular activity measures, e.g. due to any potential arousal or exploratory differences between the two groups.

Regions of interest and histological targets

The present study investigated the relationships between overt amyloid pathology in the retrosplenial cortex (β-amyloid$_{(1-42)}$ deposition and Congo Red staining) and changes in cellular activity. While the primate posterior cingulate region contains areas 23, 29, 30, and 31, in rats and mice only the retrosplenial cortex (areas 29 and 30) is present (Vogt, 1993). For comparison purposes cortical tissue from the primary visual cortex was studied. The primary visual cortex was selected as although it shows abundant amyloid in APP+ and double transgenic PSAPP mice (Reiman et al., 2000; Valla et al., 2006), the hypometabolism observed in imaging studies of Alzheimer's disease preferentially targets the retrosplenial cortex rather than the primary visual cortex.

Histological methods

Production of c-Fos protein is up-regulated by a wide variety of stimuli and conditions (Herdegen and Leah, 1998; Herrera and Robertson, 1996; Hughes et al., 1999; Tischmeyer and Grimm, 1999) and often peaks around 90 minutes after stimulation (Chaudhuri, 1997). This interval was, therefore, selected between placing the mice in a novel context and irreversibly anesthetizing the mouse with sodium pentobarbital (Euthatal, Rhone Merieux, UK). The mice were then perfused transcardially with 0.1 M PBS followed by 4% paraformaldehyde in 0.1 M PBS (PFA). The brains were removed and post-fixed in PFA for two hours and then transferred to 25% sucrose overnight. Sections were cut coronally at 20 μm on a freezing microtome. Adjacent series were collected and stored at −20°C in cryoprotectant solution until processing for Congo Red and Nissl staining, cytochrome oxidase staining, and immunohistochemical visualization of c-Fos protein and β-amyloid peptides. Tissues for both conditions (transgenic and wildtype) were processed together at each time point to reduce between-group variance. Series of sections for all four markers were then mounted on gelatinized slides, dehydrated through a series of alcohol gradients, and coverslipped.

c-Fos and β-amyloid$_{(1-42)}$ immunohistochemistry—Acute changes in the activity of neuronal systems are revealed by c-Fos labeling (Herrera and Robertson, 1996) whereas cytochrome oxidase reflects longer-term energy metabolism, in comparison to measures of

glucose consumption that indicate acute energy metabolism changes (Wong-Riley, 1989). Unless stated otherwise, all solutions were made either in 0.1 M phosphate-buffered saline (PBS, pH 7.4) containing 0.2% Triton X-100 (PBST) for c-Fos, or in 0.1 M Tris-buffered saline (TBS, pH 7.4) containing 0.1% Triton X-100 (TXTBS) for β-amyloid$_{(1-42)}$. Washes were done in PBST for c-Fos and TBS for β-amyloid$_{(1-42)}$. The β-amyloid$_{(1-42)}$ protocol first involved incubation of sections in 85% formic acid in distilled water for 10 minutes at 25°C, followed by a TBS rinse. Endogenous peroxidase activity was blocked for β-amyloid$_{(1-42)}$ sections by incubating the sections for five minutes in distilled water with 0.3 % hydrogen peroxide and also 10% methanol. c-Fos sections were blocked with 0.3 % hydrogen peroxide in PBST for ten minutes, and then all sections were rinsed four times with detergent solution alone (PBST or TXTBS, accordingly) for the same duration. The β-amyloid$_{(1-42)}$ protocol additionally included a step with 3 % normal goat serum in TXTBS for one hour. Sections were next incubated in detergent solution with rabbit polyclonal antibody at 4°C for 48 hours for c-Fos (1:5000, Ab-5, Oncogene Science, Cambridge, USA) or overnight at room temperature on a shaker for β-amyloid$_{(1-42)}$ (1:5000, AB5078P, Chemicon, Temecula, CA). Sections were then rinsed for either in PBST or TBS, accordingly. Next they were incubated in biotinylated secondary antibody (Vector Laboratories, Orton Southgate, UK), and then avidin-biotinylated horseradish peroxidase complex in PBST (c-Fos, Elite Kit, Vector Laboratories, Peterborough, UK; β-amyloid$_{(1-42)}$, Dako, Ely, UK). Sections were then rinsed in Tris non-saline buffer (TNS, pH 7.4). Finally, immunoreactivity was visualized with diaminobenzidine (DAB Substrate Kit, Vector Laboratories) chromogen incubation.

β-amyloid$_{(4-10)}$, immunohistochemistry—In view of the potential importance of the earliest age group for determining chronological progression, further analyses were conducted [5-month old transgenic group (*n*=8), as well as a sample from the 17-month old group (*n*=4)] using a human APP/ Aß- specific antibody directed against amino acid residues 4-10 of β-amyloid, W0-2 (Ida et al., 1996) for total levels. As it has recently been argued that the standard formic acid approach (also used in this study) for visualization of amyloid with β-amyloid$_{(1-42)}$ immunohistochemistry may be slightly insensitive, a recommended heating pre-treatment was used (Christensen et al., 2009; D'Andrea et al., 2003; Ohyagi et al., 2007).

The procedures for visualization of β-amyloid$_{(4-10)}$ were generally similar to those described above for β-amyloid$_{(1-42)}$ labeling, except that sections were 1) pre-treated in citrate solution, instead of formic acid, for 30 minutes at 85°C; 2) incubated in primary antibody (W0-2, The Genetics Company, Schlieren, Switzerland, 1:12 000 in TXTBS) overnight (~18 hours); and 3) after the final TXTBS rinse, the protocol proceeded straight to the DAB step.

Cytochrome oxidase histochemistry—An adjacent series of sections was washed in TNS to remove the cryoprotectant and then incubated in pre-warmed (37°C) medium comprising 0.56 g/ml DAB, 0.28 g/ml cytochrome C (C2506, Sigma, Poole, Dorset, UK) and 0.44 g/ml sucrose in TNS for approximately 40 minutes. The reaction was stopped by three washes of the sections in TNS for five minutes each, which were then left overnight.

Congo Red—Congo Red (Bio-Optica, Milan, Italy) staining according to the Highman method proceeded according to the manufacturer's protocol, except the counterstaining step, which used cresyl violet. Briefly, the sections were rinsed in distilled water, followed by a 15 min incubation in Congo Red solution. After rinsing, an alkaline differentiation buffer was left to act for 30s. Washed in tap water for 5 min, the sections were left in a phosphate buffer solution for 2 min, and finally stained with cresyl violet.

Image capture and analyses

Sections were viewed on a Leica DMRB microscope, photographed using an Olympus DP70 camera, and transferred to a computer. Quantifications were carried out using the program analySIS^D (Olympus, UK). The detection threshold was set automatically, at the same level for all sections from a same processing batch, based on overall illumination across both hemispheres. For the optical density of cytochrome oxidase, grayscale images were white balanced (i.e. normalized) using adjacent white matter on the same section (corpus callosum) as an additional control for variations in the intensity of the enzymatic reaction. Amyloid loading with age was determined by obtaining the percentage of the area of the region of interest covered by label, separately for β-amyloid(1-42) and Congo Red. Measures were made in a frame area of 1768 × 1331 μm, using 5× magnification. The camera was positioned so that counts comprised all layers of retrosplenial granular cortex b. Separate counts were taken for the superficial laminae (layer II to top of III, note there is no c-Fos label in Rgb lamina I), and the deep laminae (deep III to VI). The rationale for this lamina distinction came from evidence of differential laminar amyloid deposition in a double transgenic mouse model (van Groen et al., 2006) and from the finding that the activity of the superficial Rgb laminae can be far more sensitive to thalamic deafferentation than the deep laminae (Jenkins et al., 2004; Poirier et al., 2008).

While the Tg2576 line of transgenic mice is thought to exhibit no retrosplenial cortex neuronal loss (Ribé et al., 2005; Stack et al., 2006), any gross atrophy of the retrosplenial cortex in the transgenic cohorts would compromise any findings. For this reason, the area of the laminae of the retrosplenial cortex regions and the area of the primary visual cortex were measured on coronal sections (using the cytochrome oxidase series).

Measures were typically taken from three consecutive sections from both hemispheres to provide separate counts for the rostral Rgb and caudal Rgb. Counts were taken from representative sections throughout the length of the retrosplenial cortex. The rostral Rgb measures were placed approximately between −0.94 and −2.46 from bregma, while the caudal Rgb measures were between −2.7 and −4.2 from bregma (Paxinos and Franklin, 2001). The primary visual cortex measures were taken at the same level as those for caudal Rgb cortex. For all three sites, six individual counts (three per hemisphere) were averaged to produce a mean for each measure.

For the purpose of determining the potential contribution of early pathology in sites projecting to the retrosplenial cortex (van Groen et al., 1993; Vogt et al., 1987; Wyss and van Groen, 1992), measures of β-amyloid$_{(4\text{-}10)}$ label intensity were also similarly obtained for the hippocampus (between −1.3 and −2.3 mm from bregma), the anterior thalamic nuclei

(between −0.4 and −0.8 mm from bregma, comprising the anterior medial, anterior ventral and anterior dorsal nuclei), and entorhinal cortex (between −2.7 and −4.2 from bregma).

Data analyses

The data were first placed into one of two categories, namely measures of amyloid deposition (β-amyloid$_{(1-42)}$ and Congo Red) or measures of cellular activity (c-Fos and cytochrome oxidase). Measures of amyloid pathology only involved the transgenic mice (as the wild type scores were at floor levels), while cellular activity markers involved both wild-type and transgenic mice. Statistical comparisons were based on these two categories (amyloid or activity), and so an ANOVA for each category of marker was computed separately, and comparisons between markers *within* a category are presented where appropriate.

In order to 1) reduce the confounding effects of potential intensity variations with batches of cytochrome oxidase histochemistry on age group comparisons, and 2) enable direct comparisons between the two measures of cellular activity, data for c-Fos and cytochrome oxidase, which are measured using different units, were transformed to standardized values (Z-transformations per age group).

Separate analyses were carried out for the three regions of interest (rostral Rgb, caudal Rgb, primary visual cortex). Each ANOVA, therefore, comprised the variables of Age (5, 11, 17, and 23 months), as well as Marker (two levels: β-amyloid$_{(1-42)}$ and Congo Red; or c-Fos and cytochrome oxidase). In addition, for retrosplenial cortex subregions, there was the additional factor of Laminae (superficial and deep). The factor APP condition (two levels, wild-type and APP+ genotype) was only included for c-Fos and cytochrome oxidase analyses, as the wild-type subjects could not meaningfully be included for the analyses of pathology (amyloid) markers. Subsequently, simple effects analyses or pairwise comparisons followed where appropriate, with multiple testing adjustments (Sidak) to the significant alpha level of 0.05. The SPSS 14.0 (Chicago) statistical package was used for all analyses.

Analyses of β-amyloid$_{(4-10)}$ labeling in 5-month old Tg2576 mice comprised two stages. First, paired t-tests were used to compare the label intensity between superficial and deep laminae of the (rostral) retrosplenial cortex. Next, a multivariate statistical analysis was conducted to help evaluate whether retrosplenial cortex dysfunction might be influenced by pathology that is intrinsic to Rgb or is located in afferent regions. A path model using the statistical package Amos 17.0 (Crawfordville, USA) for structural equation modeling based on maximum likelihood estimation was derived. This approach takes into account individual variations, and enabled the estimation of the selective contribution to retrosplenial cortex function (rostral Rgb c-Fos activity) of local versus extrinsic sources of β-amyloid$_{(4-10)}$ pathology. This analysis thus focused on measures of rostral Rgb c-Fos activity together with the values of overall, rostral Rgb β-amyloid$_{(4-10)}$ immunostaining with those of the adjacent rostral hippocampus (HPC) and of the anterior thalamic nuclei (anterior dorsal, anterior ventral, and anterior medial; ATN) in 5 month old mice. We accepted the model as a satisfactory representation of the data when exhibiting a non-significant chi-square (χ^2), a

comparative fit index (CFI) value of ≥0.95, and a root mean square of approximation (RMSEA) that was not significantly greater than 0.05.

Results

Behavioral reactivity to the novel environment

Importantly for the following analyses of brain activation, there were no statistically significant effects of genotype on locomotor reactivity to the novel environment [Age × APP, F(3,50)=1.84, *p*=0.15; Age, F(3,50)=1.48, *p*=0.23; all other effects, F<1].

Histology

For very occasional subjects the histological quality of a particular marker at a specific brain level proved to be unacceptable and so the case was exclude prior to formal counting procedures. Table 1 gives the total number of cases used for each comparison. First, analyses of the area of the regions of interest (Table 2) revealed no apparent macroscopic atrophy (i.e. no changes in total area) with Age or APP+ condition for rostral retrosplenial cortex (each F<1, likewise for all possible interactions) as well as for caudal retrosplenial cortex [Age, F(3,44)=1.4, p>0.26; APP+ condition, F(1,44)=2.3, p>0.13; interactions of Laminae or Age with APP+, F<1). The analyses for the visual cortex area also revealed no area change with APP mutation (F<1) and, while there was a reduction in the area of this region with Age [F(3,42)=3.5, p<0.05], there was no interaction of Age and APP mutation [F(3,42)=1.8, p>0.15]. These findings help to preclude the possibility that group comparisons were confounded by macroscopic regional atrophy.

Regional analyses of time course of neuropathology and cellular activity measures

Rostral retrosplenial (Rgb) cortex

Amyloid pathology (β-amyloid$_{(1-42)}$ and Congo Red-positive material): β-amyloid$_{(1-42)}$ immunoreactive material was first visible in small numbers in the hippocampal formation and some cortical areas in 11-month old Tg2576 mice (see arrow in Figure 1, potentially a pre-mature presentation of cored plaques). The APP mutation led to the appearance of abundant diffuse amyloid accumulation in the retrosplenial cortex in old (17-23 month) Tg2576 mice. The two amyloid markers provided slightly different patterns of deposition in rostral Rgb (Figs. 1 and 3A) in 17- and 23-month old mice. Amyloid coverage labeled with β-amyloid$_{(1-42)}$ was overall more extensive than the congophilic (Congo Red) plaque form [F(1,23)=36.4, *p*<0.001], and increased more with age [overt pathology Marker × Age, F(3,23)=16.6, *p*<0.001].

The superficial laminae exhibited a greater abundance of coverage by overall amyloid deposition (β-amyloid$_{(1-42)}$ and Congo Red-positive material) than the deep laminae [Laminae × Age, F(3,23)=10.2, *p*<0.05]. This superficial laminae preference was visible from the first signs of amyloid deposition in the retrosplenial cortex [at 17 months, F(1,23)=5.6, *p*<0.05; adjusted for multiple comparisons; superficial, M=2.316% area covered, SE=0.607; deep, M=0.736%, SE=0.530, *p*<0.05; and also at 23 months, F(1,23)=11.2, *p*<0.005; superficial, M=5.641%, SE=0.718; deep, M=2.990%, SE=0.628,

$p<0.005$; for both younger age groups, F<1], and was largely attributable to the pattern of β-amyloid$_{(1-42)}$ rather than Congo Red-positive coverage, as seen in Figure 3A [Marker × Laminae interaction, F(1,23)=26.7, $p<0.005$; β-amyloid$_{(1-42)}$ coverage more extensive in superficial than deep laminae [F(1,23)=10.4, $p<0.005$; but there was no overall laminar difference for Congo-positive material (F<1).

c-Fos and cytochrome oxidase: These two activity markers gave strikingly different profiles of activity across age groups in rostral Rgb (Figs. 2 and 4A). Compared with wild-type mice, Tg2576 mice showed a relative increase in c-Fos activity with age. In contrast, cytochrome oxidase activity is elevated at 5 months of age in Tg2576 mice, compared to the wild-type mice. These opposite patterns of cellular activity for the wild-type and the transgenic mice were confirmed by a significant three-way interaction [Fig. 4A, cellular activity Marker × Age × APP condition, F(3,51)=6.095, $p<0.005$; all other effects, $p>0.30$]. At 5 months, Tg2576 mice exhibited less c-Fos than their wild-type siblings [F(1,51)=5.6, $p<0.05$], but more intense cytochrome oxidase activity [F(1,51)=4.7, $p<0.05$]. However, by 23 months, Tg2576 mice displayed greater c-Fos levels than the wild type mice, F(1,51)=4.3, $p<0.05$]. There was no difference for cytochrome oxidase at this age F(1,51)=1.6, $p=0.217$], nor any differences in the intermediate age groups for either c-Fos or cytochrome oxidase (all F<1). Moreover, there were no other significant main effects or any significant interactions for the functional markers, notably laminae differences [all $p > 0.34$], unlike β-amyloid$_{(1-42)}$.

Caudal retrosplenial (Rgb) cortex: The patterns found for the caudal portion of Rgb were similar to those found for rostral Rgb, and so only differential patterns are detailed below.

Amyloid pathology (β-amyloid$_{(1-42)}$ and Congo Red-positive material): Superficial laminae preference for overall amyloid deposition was maintained in the caudal Rgb, yet only emerged in the oldest 23 month old mice, and was delayed relative to the 17-month pattern for rostral Rgb [Laminae × Age, F(3,23)=18.0, p<0.001; 23 months, F(1,23)=67.4, p<0.001; all other Age group laminar comparisons $p>0.12$; see Fig. 3B]. Yet, in contrast to rostral Rgb, Congo Red-positive plaques appeared more substantially in the deep laminae [F(3,23)=3.0, $p=0.05$].

c-Fos and cytochrome oxidase: Although the overall patterns for caudal Rgb resembled those for rostral Rgb (Fig. 4B), unlike the latter there were no significant main effects or any significant interactions for cellular activity measures in caudal Rgb [all F<1, except APP condition × Age, F(1,42)=1.2, $p=0.316$; Marker × APP condition, F(1,42)=1.4, $p=0.246$; Marker × APP condition × Age, F(3,42)=1.7, $p=0.18$].

Primary visual cortex

Amyloid pathology (β-amyloid$_{(1-42)}$ and Congo Red-positive material): Overall, the pattern of age of onset of β-amyloid$_{(1-42)}$ deposition in the primary visual cortex was similar to that found for both retrosplenial cortex subregions, although the final accumulation of Congo-positive material was more extensive in the primary visual cortex (see Fig. 3C). Overall amyloid burden increased with age, but this increase only reached statistical significance by

23 months (area coverage; 23 m, M=3.9%, SE=0.81; 5 m, M<0.0 E-15%, SE=0.61, p=0.005; 11 m, M=0.14%, SE=0.74, p<0.05; 17 m, M=0.90, SE=0.64, p<0.05; all other comparisons p>0.89).

Like caudal Rgb, there was a greater percent area coverage in primary visual cortex by β-amyloid$_{(1-42)}$ than Congo Red, but this difference was only significant at 23 months (respectively, M=6.8% area coverage, SE=0.16;M=0.9%, SE=0.14, p<0.005; all other comparisons p>0.17).

c-Fos and cytochrome oxidase: As seen in Figure 4C, the only significant transgenic effect in the primary visual cortex was the interaction between cellular activity Marker and genotype [F(1,39)=6.6, p<0.05]. Subsequent analyses confirmed that this interaction reflected more intense cytochrome activity in Tg2576 mice than their wildtype siblings [F(1,39)=7.3, p<0.05], but no overall difference between these groups for c-Fos expression F(1,39)=1.3, p=0.262]. There were no other significant main effects or any significant interactions [all F<1, except APP condition × Age, F(1,39)=1.7, p=0.184].

Retrosplenial cortex dysfunction with local and distal initial APP processing

Early presence of mutated APP-derived peptides: In order to investigate further the cellular activity dysfunction already exhibited by the young, 5-month old mice, prior to the appearance of overt amyloid accumulation, additional immunohistochemical analyses were conducted using an alternative marker [W0-2, β-amyloid$_{(4-10)}$] and pretreatment. Omission of the formic acid pre-treatment yielded only very light cellular marking (not shown), markedly less intense than that seen after citric acid pre-treatment. Young (5 month, n = 8) transgenic mice exhibited a predominantly cellular-looking W0-2 accumulation in the retrosplenial cortex. In contrast to β-amyloid$_{(1-42)}$, there was no particular retrosplenial cortex laminar preference for this label (Fig. 5; all comparisons p > .12). Furthermore, this cellular pattern appeared to be transient as it was absent in the older, 17-month old Tg2576 mice (n=4). At this age, the appearance, laminar distribution pattern, and abundance (see Fig. 5) appeared equivalent between β-amyloid$_{(4-10)}$ and β-amyloid$_{(1-42)}$, just as observed for caudal retrosplenial cortex and primary visual cortex labeling.

Impact of local and distal APP(swe)-derived peptides on retrosplenial cortex (Rgb) function: In conjunction with the earlier appearance of β-amyloid$_{(1-42)}$ in the extended hippocampal system than the retrosplenial cortex than (see Fig. 1 for an example), the presence of β-amyloid$_{(4-10)}$ was always accompanied by labeling in regions such as the hippocampus, the anterior thalamus, and the entorhinal cortex, which all project strongly to the retrosplenial cortex and β-amyloid$_{(1-42)}$. In order to evaluate the importance of the source (intrinsic vs. extrinsic) of the pathological seeding in influencing early, pre-amyloid retrosplenial cortex dysfunction, multivariate statistical analyses were conducted using data from the 5-month old transgenic mice. This approach revealed selective associations of retrosplenial, anterior thalamic and hippocampal W0-2 [β-amyloid$_{(4-10)}$] staining with retrosplenial cortex activity disturbances (model with good fit; χ^2 = 0.82, df = 2, p > 0.9; CFI = 1.00; RMSEA < .001, p > 0.9). Specifically, after removing non-significant relationships with retrosplenial cortex measures (p > 0.5), the parsimonious model shown in Figure 6

describes how intrinsic and extrinsic pathology were associated with retrosplenial cortex function. Retrosplenial cortex W0-2 levels appeared to be strongly linked to those of the anterior thalamus ($p < 0.001$), but not the rostral hippocampal ($p = 0.11$; not shown]. Separate consideration of the anterior thalamic nuclei revealed that the predictive ability of the anterodorsal nucleus for retrosplenial cortex pathology by was relatively stronger than the anterodorsal nucleus, and that of the anteroventral nucleus was not significant; not shown).

In turn, retrosplenial cortex c-Fos activity could be significantly predicted by W0-2 levels found both within [$Rgb_{(rostral)}$ β-$amyloid_{(4-10)}$, $p < 0.05$] and also afferent [$HPC_{(rostral)}$ β-$amyloid_{(4-10)}$, $p < 0.005$] to the retrosplenial cortex. Finally, the W0-2 levels observed in the entorhinal cortex, another source of strong Rgb projections, did not significantly relate to the retrosplenial patterns (data not shown), suggesting that only selective retrosplenial cortex afferents contribute to its dysfunction.

Discussion

Extending earlier observations of APP+ mice (van Groen et al., 2006), this study described the progression of amyloid accumulation in the retrosplenial cortex along with metabolic and neuronal signaling markers of cellular function. The target region, the retrosplenial cortex, is increasingly thought to play an important role in Alzheimer's disease (Nestor et al., 2003a; Nestor et al., 2003b; Vann et al., 2009), while rodent studies reinforce the view that this cortical area is critical for normal memory (reviewed in Aggleton, 2009; Vann et al., 2009). At the same time, the location and size of the human retrosplenial cortex pose particular problems for research (Vann et al., 2009), so supporting the comparative approach.

A key finding of the present study was that young Tg2576 mice showed aberrant changes of two markers of cellular activity in the retrosplenial cortex (particularly rostral Rgb, 5 months) well before the formation of overt congophilic and β-$amyloid_{(1-42)}$–labeled plaques. As expected (Hsiao et al., 1996; Kawarabayashi et al., 2001), β-$amyloid_{(1-42)}$ immunoreactive material was first visible in small numbers in the hippocampal formation and some cortical areas in 11-month old Tg2576 mice (Figure 1). The APP mutation led to the appearance of abundant diffuse amyloid accumulation in the retrosplenial cortex in old (17-23 month) Tg2576 mice, as has been previously seen in double transgenic PS1/APP and triple transgenic PS1/APP/Tau mice (Robertson et al., 2009; van Groen et al., 2003). Yet pre-amyloidosis disturbances were observed in the younger, 5-month old mice. At this early stage of pathology, the presence of mutant APP and -derived species both intrinsic and extrinsic to the retrosplenial cortex could jointly predict a significant proportion of aberrant cellular, c-Fos reactivity. The temporal dissociation between the appearance of cellular dysfunction and amyloid plaque deposition, together with evidence of discordance between the extent of hypometabolism and atrophy in posterior cingulate cortex in Alzheimer's disease (e.g. Chételat et al., 2008; Chételat et al., 2009), emphasize the sensitivity of the retrosplenial cortex to early pathological processes linked to APP processing.

Young Tg2576 mutant mice are an informative model with which to evaluate the effects of APP pathology on retrosplenial cortex as they appear to be largely free from cell loss and atrophy confounds, as well as from neuropil threads seen in humans and certain alternative murine models of Alzheimer's disease (Borg and Chereul, 2008; Ribé et al., 2005; Stack et al., 2006). Tg2576 mice are thought to model the very early stages of amyloid pathology, and as they do not show extensive cell loss, the deficits more likely reflect impairments in synaptic function and associated reductions in dendritic spine density, as well as disturbed mitochondrial function that occur prior to plaque formation (e.g. Jacobsen et al., 2006; Lanz et al., 2003; Schmidt et al., 2008). The W0-2 primary antibody [β –amyloid$_{(4-10)}$]used in the current study enabled the visualization at 5 months of the total APP-derived peptides. In the absence of β-amyloid$_{(1-42)}$ at this age, the cellular activity disturbances associated with the W0-2 binding levels may thus implicate, in addition to human but not murine, APP, various uncleaved or cleaved (α, β, or γ-secretase) C-terminal fragments, as well as diverse other β-amyloid species (e.g. Beher et al., 2002; Munter et al., 2007; Rutten et al., 2003). Our findings (Fig. 5) support the view that pathology precedes extracellular amyloid plaque aggregation (Hardy and Selkoe, 2002; Walsh and Selkoe, 2004), providing evidence of such an early form of dysfunction in the vulnerable retrosplenial cortex.

β-amyloid$_{(1-42)}$ is associated with synaptic dysfunction (Dong et al., 2007; Spires-Jones et al., 2007; Stern et al., 2004; Takahashi et al., 2002) and reduced immediate-early gene activity (Dickey et al., 2003; Palop et al., 2005; Palop et al., 2003) in the hippocampus and various cortical areas in Alzheimer's mouse models. As such, it was expected that retrosplenial cortex c-Fos levels in the current study would exhibit dramatic reductions with the local appearance of amyloid plaque deposition. However, a main finding of the current study is that while retrosplenial c-Fos activity was decreased in the presence of an early form of pathology [labeled with β-amyloid$_{(4-10)}$ antibody], it thereafter *increased* with the appearance of overt amyloid plaques [congophilic or β-amyloid$_{(1-42)}$].

The different effects of early and later emerging pathology may be related to direct effects of APP and β-amyloid on mitochondrial function (Ferrer, 2009). Cytochrome oxidase levels are reduced in the posterior cingulate region in Alzheimer's disease (Liang et al., 2008a; Liang et al., 2008b; Valla et al., 2001), potentially due to the effects of APP and its derivative β-amyloid, targeting mitochondria and causing their dysfunction (Anandatheerthavarada et al., 2003). Bearing in mind that c-Fos itself may be induced by antioxidants rather than oxidants (Meyer et al., 1993), its level in rostral Rgb is consistent with the pattern of amyloidosis-associated oxidative activity (Manczak et al., 2005; Reddy et al., 2004). In this light, because c-Fos is capable of binding to mitochondrial DNA (Ogita et al., 2003; Ogita et al., 2002), it is plausible that its increasing levels with age could relate to antioxidant mechanisms. The elevation in cytochrome oxidase activity in the young transgenic mice may reflect an early peak of oxidative pathology, as seen in Alzheimer's disease (Petersen et al., 2007). Likewise, Strazielle and colleagues (2003) reported upregulated mitochondrial metabolism in the hippocampus and anterior cortical regions in 16-month old APP(swe)751 mice (Strazielle et al., 2003), similar to that observed in the hippocampus and cortex of Tg2576 mice up to 18 months of age, followed by a reduction at 24 months of age (Manczak et al., 2005; Reddy et al., 2004). Overall, the opposite levels of

c-Fos and cytochrome oxidase (Conejo et al., 2007; Salin et al., 2002) in the retrosplenial cortex of 5-month old Tg2576 mice support the notion that amyloid species generation diminishes cellular efficiency and provokes an increased energy expenditure (Allaman et al., 2010; Bayer and Wirths, 2010; Ferrer, 2009).

The current study suggests that in addition to local effects, early mutant APP-derived pathology in selective afferents of the retrosplenial cortex may also contribute to retrosplenial dysfunction (Figs. 5, 6). The contrasting association with hippocampal pathology (Fig. 6) could potentially implicate disruptions of vulnerable direct inhibitory hippocampal projections (González et al., 2008; Jinno et al., 2007; Miyashita and Rockland, 2007; Perez et al., 2010), opposite to excitatory anterior thalamic input (Gonzalo-Ruiz et al., 1997; Wang et al., 2001).

It is notable that distal lesions in the anterior thalamus and the hippocampus induce retrosplenial cortex immediate-early gene deficits, and that anterior thalamic nuclei lesions produce widespread retrosplenial cortex transcriptome alterations that include reductions in energy function, all of which are unaccompanied by cell loss or atrophy (Albasser et al., 2007; Jenkins et al., 2004; Poirier et al., 2008). The functional impact of these distal lesion effects is revealed by the discovery that anterior thalamic lesions disrupt the behavioural training-induced discriminative electrophysiological activity and bring about a loss of retrosplenial plasticity (Gabriel et al., 1983; Garden et al., 2009). Moreover, infusion of amyloid fragments into the anterior thalamic nuclei reduces neurotransmitter levels in the retrosplenial cortex (Gonzalo-Ruiz, 1999). In contrast, entorhinal cortex lesions and mutant APP-derived pathology affect neither retrosplenial cortex immediate-early gene activity (Albasser et al., 2007; current study) nor diffuse amyloid deposition (Sheng et al., 2002). The progression of overt pathology in Alzheimer's disease has been divided into six stages (Braak and Braak, 1991b). While the entorhinal cortex appears to show the most severe pathology in the earliest stages, which may be below the threshold for clinical symptoms, by Stage III there is additional involvement of the hippocampal formation and the anterior thalamic nuclei (Braak and Braak, 1991a; Braak and Braak, 1993).

The evidence described expands on the view that distal pathology is important for driving early disturbances in posterior cingulate function in the course of Alzheimer's disease (Aupée et al., 2001; Chételat et al., 2003; Chételat et al., 2008; Garrido et al., 2002; Hirao et al., 2006; Matsuda, 2001; Matsuda et al., 2002; Meguro et al., 1999; Minoshima et al., 1997; Nestor et al., 2003a; Rémy et al., 2005; Villain et al., 2008; Villain et al., In Press), even in the absence of atrophy. This notion is further supported by evidence of pathology at prodromal stages in those pathways that project to the retrosplenial cortex (Fellgiebel et al., 2008; Xie et al., 2006; Zhang et al., 2007; Zhou et al., 2008). Dysfunction in turn may spread throughout the network, as suggested by the demonstrations that infusions of amyloid species into the retrosplenial cortex can have downstream effects (Arevalo-Serrano et al., 2008; González et al., 2008; González et al., 2007; Gonzalo-Ruiz and Arévalo-Serrano, 2006; Gonzalo-Ruiz and Sanz, 2002; Perez et al., 2010).

In conclusion, out data provide novel insights into the pattern of cortical and subcortical cellular changes during aging in Tg2576 mice. Our results provide evidence for early

metabolic abnormalities in the retrosplenial cortex. Furthermore, these cellular changes are related to pathological changes in the hippocampus and the anterior thalamus. These data confirm that early changes in functional activity in the retrosplenial cortex may provide a useful marker in conjunction with cognitive and imaging methods for AD progression and drug intervention studies in both human and animal studies.

Acknowledgments

This research was funded by the Alzheimer's Research Trust (UK, grant ART/PPG2005B/7). We wish to thank Dr. Mariah Lelos, Dr. Thomas van Groen, and Dr. Inga Kadish, for their technical assistance, and the anonymous reviewers for their helpful comments.

References

Aggleton JP. EPS Mid-Career Award 2006. Understanding anterograde amnesia: disconnections and hidden lesions. Q J Exp Psychol. 2008; 61:1441–71.

Aggleton JP. Understanding retrosplenial amnesia: Insights from animal studies. Neuropsychologia. 2009

Albasser MM, et al. Hippocampal lesions halve immediate-early gene protein counts in retrosplenial cortex: distal dysfunctions in a spatial memory system. Eur J Neurosci. 2007; 26:1254–1266. [PubMed: 17767503]

Allaman I, et al. Amyloid-{beta} Aggregates Cause Alterations of Astrocytic Metabolic Phenotype: Impact on Neuronal Viability. J. Neurosci. 2010; 30:3326–3338. [PubMed: 20203192]

Anandatheerthavarada HK, et al. Mitochondrial targeting and a novel transmembrane arrest of Alzheimer's amyloid precursor protein impairs mitochondrial function in neuronal cells. J. Cell Biol. 2003; 161:41–54. [PubMed: 12695498]

Arevalo-Serrano J, et al. Beta-amyloid peptide-induced modifications in alpha7 nicotinic acetylcholine receptor immunoreactivity in the hippocampus of the rat: relationship with GABAergic and calcium-binding proteins perikarya. Brain Res Bull. 2008; 75:533–44. [PubMed: 18355629]

Aupée AM, et al. Voxel-based mapping of brain hypometabolism in permanent amnesia with PET. NeuroImage. 2001; 13:1164–1173. [PubMed: 11352622]

Bayer TA, Wirths O. Intracellular accumulation of amyloid-beta - a predictor for synaptic dysfunction and neuron loss in Alzheimer's disease. Frontiers in Aging Neuroscience. 2010; 2

Beher D, et al. Generation of C-terminally truncated amyloid-β peptides is dependent on γ-secretase activity. Journal of Neurochemistry. 2002; 82:563–575. [PubMed: 12153480]

Borg J, Chereul E. Differential MRI patterns of brain atrophy in double or single transgenic mice for APP and/or SOD. J Neurosci Res. 2008; 86:3275–3284. [PubMed: 18646206]

Braak H, Braak E. Alzheimer's disease affects limbic nuclei of the thalamus. Acta Neuropathol. 1991a; 81:261–8. [PubMed: 1711755]

Braak H, Braak E. Neuropathological stageing of Alzheimer-related changes. Acta Neuropathol. 1991b; 82:239–59. [PubMed: 1759558]

Braak, H.; Braak, E. Alzheimer neuropathology and limbic circuits. In: Vogt, BA.; Gabriel, M., editors. Neurobiology of Cingulate Cortex and Limbic Thalamus: A Comprehensive Handbook. Birkhäuser; Boston: 1993. p. 606-626.

Buckner RL, et al. Molecular, Structural, and Functional Characterization of Alzheimer's Disease: Evidence for a Relationship between Default Activity, Amyloid, and Memory. J. Neurosci. 2005; 25:7709–7717. [PubMed: 16120771]

Chapman PF, et al. Impaired synaptic plasticity and learning in aged amyloid precursor protein transgenic mice. Nat Neurosci. 1999; 2:271–6. [PubMed: 10195221]

Chaudhuri A. Neural activity mapping with inducible transcription factors. Neuroreport. 1997; 8:iii–viii. [PubMed: 9376510]

Chételat G, et al. Dissociating atrophy and hypometabolism impact on episodic memory in mild cognitive impairment. Brain. 2003; 126:1955–1967. [PubMed: 12821520]

Chételat G, et al. Direct voxel-based comparison between grey matter hypometabolism and atrophy in Alzheimer's disease. Brain. 2008; 131:60–71. [PubMed: 18063588]

Chételat G, et al. Posterior cingulate hypometabolism in early Alzheimer's disease: what is the contribution of local atrophy versus disconnection? Brain. 2009; 132:e133. author reply e134. [PubMed: 19858081]

Christensen DZ, et al. Formic acid is essential for immunohistochemical detection of aggregated intraneuronal A[beta] peptides in mouse models of Alzheimer's disease. Brain Research. 2009; 1301:116–125. [PubMed: 19751708]

Conejo NM, et al. Brain c-Fos immunocytochemistry and cytochrome oxidase histochemistry after a fear conditioning task. Psicothema. 2007; 19:295–301. [PubMed: 17425902]

D'Andrea MR, et al. The use of formic acid to embellish amyloid plaque detection in Alzheimer's disease tissues misguides key observations. Neuroscience Letters. 2003; 342:114–118. [PubMed: 12727331]

Dickey CA, et al. Selectively Reduced Expression of Synaptic Plasticity-Related Genes in Amyloid Precursor Protein + Presenilin-1 Transgenic Mice. J. Neurosci. 2003; 23:5219–5226. [PubMed: 12832546]

Dong H, et al. Spatial relationship between synapse loss and beta-amyloid deposition in Tg2576 mice. J Comp Neurol. 2007; 500:311–321. [PubMed: 17111375]

Fellgiebel A, et al. Functional relevant loss of long association fibre tracts integrity in early Alzheimer's disease. Neuropsychologia. 2008; 46:1698–706. [PubMed: 18243252]

Fennema-Notestine C, et al. Structural MRI biomarkers for preclinical and mild Alzheimer's disease. Hum Brain Mapp. 2009; 30:3238–53. [PubMed: 19277975]

Ferrer I. Altered mitochondria, energy metabolism, voltage-dependent anion channel, and lipid rafts converge to exhaust neurons in Alzheimer's disease. J Bioenerg Biomembr. 2009; 41:425–31. [PubMed: 19798558]

Fleischmann A, et al. Impaired long-term memory and NR2A-Type NMDA receptor-dependent synaptic plasticity in mice lacking c-Fos in the CNS. J. Neurosci. 2003; 23:9116–9122. [PubMed: 14534245]

Fox NC, et al. Imaging of onset and progression of Alzheimer's disease with voxel-compression mapping of serial magnetic resonance images. Lancet. 2001; 358:201–5. [PubMed: 11476837]

Gabriel M, et al. Anterior thalamic lesions and neuronal activity in the cingulate and retrosplenial cortices during discriminative avoidance behavior in rabbits. Behav Neurosci. 1983; 97:675–96. [PubMed: 6639743]

Garden DL, et al. Anterior thalamic lesions stop synaptic plasticity in retrosplenial cortex slices: expanding the pathology of diencephalic amnesia. Brain. 2009; 132:1847–57. [PubMed: 19403787]

Garrido GEJ, et al. Relation between medial temporal atrophy and functional brain activity during memory processing in Alzheimer's disease: a combined MRI and SPECT study. Journal of Neurology, Neurosurgery and Psychiatry. 2002; 73:508–516.

González I, et al. Effects of beta-amyloid peptide on the density of M2 muscarinic acetylcholine receptor protein in the hippocampus of the rat: relationship with GABA-, calcium-binding protein and somatostatin-containing cells. Neuropathol Appl Neurobiol. 2008; 34:506–22. [PubMed: 18221260]

González I, et al. Effects of β-amyloid protein on M1 and M2 subtypes of muscarinic acetylcholine receptors in the medial septum-diagonal band complex of the rat: relationship with cholinergic, GABAergic, and calcium-binding protein perikarya. Acta Neuropathol. 2007; 113:637–651. [PubMed: 17294199]

Gonzalo-Ruiz A. [Changes in neurotransmission systems after the injection of beta-amyloid protein beta (12-28) in the hypothalamus and anterior thalamus of the rat]. Rev Neurol. 1999; 28:931–41. [PubMed: 10416226]

Gonzalo-Ruiz A, Arévalo-Serrano J. Interaction between β-amyloid protein and the α7 nicotinic acetylcholine receptor in cholinergic, gabaergic and calcium-binding proteins-containing neurons in the septum-diagonal band complex of the rat. Eur J Anat. 2006; 10:127–142.

Gonzalo-Ruiz A, Sanz JM. Alteration of cholinergic, excitatory amino acid and neuropeptide markers in the septum-diagonal band complex following injections of fibrilliar β-amyloid protein into the retrosplenial cortex of the rat. Eur J Anat. 2002; 6:58–71.

Gonzalo-Ruiz A, et al. Glutamate and Aspartate Immunoreactivity in the Reciprocal Projections Between the Anterior Thalamic Nuclei and the Retrosplenial Granular Cortex in the Rat. Brain Research Bulletin. 1997; 42:309–321. [PubMed: 9043718]

Greenberg ME, et al. Stimulation of neuronal acetylcholine receptors induces rapid gene transcription. Science. 1986; 234:80–3. [PubMed: 3749894]

Hale G, Good M. Impaired visuospatial recognition memory but normal object novelty detection and relative familiarity judgments in adult mice expressing the APPswe Alzheimer's disease mutation. Behav Neurosci. 2005; 119:884–91. [PubMed: 16187817]

Hardy J, Selkoe DJ. The amyloid hypothesis of Alzheimer's disease: progress and problems on the road to therapeutics. Science. 2002; 297:353–6. [PubMed: 12130773]

Herdegen T, Leah JD. Inducible and constitutive transcription factors in the mammalian nervous system: control of gene expression by Jun, Fos and Krox, and CREB/ATF proteins. Brain Res Brain Res Rev. 1998; 28:370–490. [PubMed: 9858769]

Herrera DG, Robertson HA. Activation of c-fos in the brain. Progress in Neurobiology. 1996; 50:83–107. [PubMed: 8971979]

Hirao K, et al. Functional interactions between entorhinal cortex and posterior cingulate cortex at the very early stage of Alzheimer's disease using brain perfusion single-photon emission computed tomography. Nuclear Medicine Communications. 2006; 27:151–156. [PubMed: 16404228]

Hsiao K, et al. Correlative memory deficits, Abeta elevation, and amyloid plaques in transgenic mice. Science. 1996; 274:99–102. [PubMed: 8810256]

Hughes PE, et al. Activity and injury-dependent expression of inducible transcription factors, growth factors and apoptosis-related genes within the central nervous system. Prog Neurobiol. 1999; 57:421–50. [PubMed: 10080384]

Iaria G, et al. Retrosplenial and hippocampal brain regions in human navigation: complementary functional contributions to the formation and use of cognitive maps. Eur J Neurosci. 2007; 25:890–899. [PubMed: 17298595]

Ida N, et al. Analysis of Heterogeneous βA4 Peptides in Human Cerebrospinal Fluid and Blood by a Newly Developed Sensitive Western Blot Assay. Journal of Biological Chemistry. 1996; 271:22908–22914. [PubMed: 8798471]

Jacobsen JS, et al. Early-onset behavioral and synaptic deficits in a mouse model of Alzheimer's disease. Proc Natl Acad Sci U S A. 2006; 103:5161–6. [PubMed: 16549764]

Jenkins TA, et al. Anterior thalamic lesions stop immediate early gene activation in selective laminae of the retrosplenial cortex: evidence of covert pathology in rats? Eur J Neurosci. 2004; 19:3291–304. [PubMed: 15217385]

Jinno S, et al. Neuronal diversity in GABAergic long-range projections from the hippocampus. J Neurosci. 2007; 27:8790–804. [PubMed: 17699661]

Kasahara J, et al. Activation of calcium/calmodulin-dependent protein kinase IV in long term potentiation in the rat hippocampal CA1 region. J Biol Chem. 2001; 276:24044–50. [PubMed: 11306573]

Kawarabayashi T, et al. Age-dependent changes in brain, CSF, and plasma amyloid (beta) protein in the Tg2576 transgenic mouse model of Alzheimer's disease. J Neurosci. 2001; 21:372–81. [PubMed: 11160418]

Lanz TA, et al. Dendritic spine loss in the hippocampus of young PDAPP and Tg2576 mice and its prevention by the ApoE2 genotype. Neurobiol Dis. 2003; 13:246–53. [PubMed: 12901839]

Liang WS, et al. Altered neuronal gene expression in brain regions differentially affected by Alzheimer's disease: a reference data set. Physiol Genomics. 2008a; 33:240–56. [PubMed: 18270320]

Liang WS, et al. Alzheimer's disease is associated with reduced expression of energy metabolism genes in posterior cingulate neurons. Proc Natl Acad Sci U S A. 2008b; 105:4441–6. [PubMed: 18332434]

Maguire E. The retrosplenial contribution to human navigation: A review of lesion and neuroimaging findings. Scand J Psychol. 2001; 42:225–238. [PubMed: 11501737]

Manczak M, et al. Time-course of mitochondrial gene expressions in mice brains: implications for mitochondrial dysfunction, oxidative damage, and cytochrome c in aging. J Neurochem. 2005; 92:494–504. [PubMed: 15659220]

Matsuda H. Cerebral blood flow and metabolic abnormalities in Alzheimer's disease. Ann Nucl Med. 2001; 15:85–92. [PubMed: 11448080]

Matsuda H, et al. Longitudinal evaluation of both morphologic and functional changes in the same individuals with Alzheimer's disease. J Nucl Med. 2002; 43:304–311. [PubMed: 11884488]

Meguro K, et al. Neocortical and hippocampal glucose hypometabolism following neurotoxic lesions of the entorhinal and perirhinal cortices in the non-human primate as shown by PET: Implications for Alzheimer's disease. Brain. 1999; 122:1519–1531. [PubMed: 10430835]

Meyer M, et al. H2O2 and antioxidants have opposite effects on activation of NF-kappa B and AP-1 in intact cells: AP-1 as secondary antioxidant-responsive factor. EMBO J. 1993; 12:2005–15. [PubMed: 8491191]

Minoshima S, et al. Metabolic reduction in the posterior cingulate cortex in very early Alzheimer's disease. Annals of Neurology. 1997; 42:85–94. [PubMed: 9225689]

Miyashita T, Rockland KS. GABAergic projections from the hippocampus to the retrosplenial cortex in the rat. Eur J Neurosci. 2007; 26:1193–204. [PubMed: 17767498]

Morgan JI, Curran T. Stimulus-transcription coupling in the nervous system: involvement of the inducible proto-oncogenes fos and jun. Annu Rev Neurosci. 1991; 14:421–51. [PubMed: 1903243]

Munter L-M, et al. GxxxG motifs within the amyloid precursor protein transmembrane sequence are critical for the etiology of A[beta]42. EMBO J. 2007; 26:1702–1712. [PubMed: 17332749]

Nestor PJ, et al. Retrosplenial cortex (BA 29/30) hypometabolism in mild cognitive impairment (prodromal Alzheimer's disease). Eur J Neurosci. 2003a; 18:2663–7. [PubMed: 14622168]

Nestor PJ, et al. Limbic hypometabolism in Alzheimer's disease and mild cognitive impairment. Ann Neurol. 2003b; 54:343–51. [PubMed: 12953266]

Nikolaev E, et al. c-fos protooncogene expression in rat hippocampus and entorhinal cortex following tetanic stimulation of the perforant path. Brain Res. 1991; 560:346–9. [PubMed: 1760742]

Ogita K, et al. Transcription factor activator protein-1 expressed by kainate treatment can bind to the non-coding region of mitochondrial genome in murine hippocampus. J Neurosci Res. 2003; 73:794–802. [PubMed: 12949905]

Ogita K, et al. Localization of activator protein-1 complex with DNA binding activity in mitochondria of murine brain after in vivo treatment with kainate. J Neurosci. 2002; 22:2561–70. [PubMed: 11923421]

Ohyagi Y, et al. Intraneuronal amyloid [beta]42 enhanced by heating but counteracted by formic acid. Journal of Neuroscience Methods. 2007; 159:134–138. [PubMed: 16860394]

Palop JJ, et al. Vulnerability of dentate granule cells to disruption of arc expression in human amyloid precursor protein transgenic mice. J Neurosci. 2005; 25:9686–93. [PubMed: 16237173]

Palop JJ, et al. Neuronal depletion of calcium-dependent proteins in the dentate gyrus is tightly linked to Alzheimer's disease-related cognitive deficits. Proc Natl Acad Sci U S A. 2003; 100:9572–7. [PubMed: 12881482]

Paxinos, G.; Franklin, KBJ. The Mouse Brain in Stereotaxic Coordinates. New York; Elesvier: 2001.

Pengas G, et al. Focal posterior cingulate atrophy in incipient Alzheimer's disease. Neurobiol Aging. 2010; 31:25–33. [PubMed: 18455838]

Perez JL, et al. Soluble oligomeric forms of beta-amyloid (Abeta) peptide stimulate Abeta production via astrogliosis in the rat brain. Exp Neurol. 2010; 223:410–21. [PubMed: 19879263]

Petersen RB, et al. Signal transduction cascades associated with oxidative stress in Alzheimer's disease. J Alzheimers Dis. 2007; 11:143–52. [PubMed: 17522439]

Poirier GL, et al. Anterior thalamic lesions produce chronic and profuse transcriptional deregulation in retrosplenial cortex: a model of retrosplenial hypoactivity and covert pathology. Thalamus Relat Syst. 2008; 4:59–77. doi: 10.1017/S1472928808000368. [PubMed: 21289865]

Reddy PH, et al. Gene expression profiles of transcripts in amyloid precursor protein transgenic mice: up-regulation of mitochondrial metabolism and apoptotic genes is an early cellular change in Alzheimer's disease. Hum Mol Genet. 2004; 13:1225–40. [PubMed: 15115763]

Reiman EM, et al. Tracking Alzheimer's disease in transgenic mice using fluorodeoxyglucose autoradiography. Neuroreport. 2000; 11:987–91. [PubMed: 10790869]

Rémy F, et al. Verbal episodic memory impairment in Alzheimer's disease: a combined structural and functional MRI study. NeuroImage. 2005; 25:253–266. [PubMed: 15734360]

Ribé EM, et al. Accelerated amyloid deposition, neurofibrillary degeneration and neuronal loss in double mutant APP/tau transgenic mice. Neurobiol Dis. 2005; 20:814–22. [PubMed: 16125396]

Robertson RT, et al. Amyloid-beta expression in retrosplenial cortex of triple transgenic mice: relationship to cholinergic axonal afferents from medial septum. Neuroscience. 2009; 164:1334–1346. [PubMed: 19772895]

Rutten BPF, et al. No alterations of hippocampal neuronal number and synaptic bouton number in a transgenic mouse model expressing the [beta]-cleaved C-terminal APP fragment. Neurobiology of Disease. 2003; 12:110–120. [PubMed: 12667466]

Salin P, et al. High-Frequency Stimulation of the Subthalamic Nucleus Selectively Reverses Dopamine Denervation-Induced Cellular Defects in the Output Structures of the Basal Ganglia in the Rat. J. Neurosci. 2002; 22:5137–5148. [PubMed: 12077209]

Schmidt C, et al. Amyloid precursor protein and amyloid beta-peptide bind to ATP synthase and regulate its activity at the surface of neural cells. Mol Psychiatry. 2008; 13:953–69. [PubMed: 17726461]

Sheng JG, et al. Disruption of corticocortical connections ameliorates amyloid burden in terminal fields in a transgenic model of Abeta amyloidosis. J Neurosci. 2002; 22:9794–9. [PubMed: 12427835]

Sheng M, Greenberg ME. The regulation and function of c-fos and other immediate early genes in the nervous system. Neuron. 1990; 4:477–85. [PubMed: 1969743]

Spires-Jones TL, et al. Impaired Spine Stability Underlies Plaque-Related Spine Loss in an Alzheimer's Disease Mouse Model. Am J Pathol. 2007; 171:1304–1311. [PubMed: 17717139]

Stack E, et al. P1-011: Neurogenesis is increased in retrosplenial cortex of six month-old Tg2576 mice. Alzheimer's and Dementia. 2006; 2:S97.

Stern EA, et al. Cortical synaptic integration in vivo is disrupted by amyloid-beta plaques. J Neurosci. 2004; 24:4535–40. [PubMed: 15140924]

Strazielle C, et al. Regional brain cytochrome oxidase activity in beta-amyloid precursor protein transgenic mice with the Swedish mutation. Neuroscience. 2003; 118:1151–63. [PubMed: 12732258]

Takahashi RH, et al. Intraneuronal Alzheimer Aß42 Accumulates in Multivesicular Bodies and Is Associated with Synaptic Pathology. Am J Pathol. 2002; 161:1869–1879. [PubMed: 12414533]

Thal DR, et al. Phases of A beta-deposition in the human brain and its relevance for the development of AD. Neurology. 2002; 58:1791–800. [PubMed: 12084879]

Tischmeyer W, Grimm R. Activation of immediate early genes and memory formation. Cell Mol Life Sci. 1999; 55:564–74. [PubMed: 10357227]

Valla J, et al. Energy hypometabolism in posterior cingulate cortex of Alzheimer's patients: superficial laminar cytochrome oxidase associated with disease duration. J Neurosci. 2001; 21:4923–30. [PubMed: 11425920]

Valla J, et al. Age- and transgene-related changes in regional cerebral metabolism in PSAPP mice. Brain Research. 2006; 1116:194–200. [PubMed: 16942758]

van Groen T, et al. Deposition of mouse amyloid beta in human APP/PS1 double and single AD model transgenic mice. Neurobiol Dis. 2006; 23:653–62. [PubMed: 16829076]

van Groen T, et al. Diffuse amyloid deposition, but not plaque number, is reduced in amyloid precursor protein/presenilin 1 double-transgenic mice by pathway lesions. Neuroscience. 2003; 119:1185–1197. [PubMed: 12831872]

van Groen, T., et al. Interconnections between the thalamus and retrosplenial cortex in the rodent brain. In: Vogt, BA.; Gabriel, M., editors. Neurobiology of Cingulate Cortex and Limbic Thalamus: A Comprehensive Handbook. Birkhäuser; Boston: 1993. p. 123-150.

van Hoesen GW, et al. Entorhinal cortex pathology in Alzheimer's disease. Hippocampus. 1991; 1:1–8. [PubMed: 1669339]

Vann SD, et al. What does the retrosplenial cortex do? Nat Rev Neurosci. 2009; 10:792–802. [PubMed: 19812579]

Villain N, et al. Relationships between hippocampal atrophy, white matter disruption, and gray matter hypometabolism in Alzheimer's disease. J Neurosci. 2008; 28:6174–81. [PubMed: 18550759]

Villain N, et al. Sequential relationships between grey matter and white matter atrophy and brain metabolic abnormalities in early Alzheimer's disease. Brain. 2010; 133:3301–3314. [PubMed: 20688814]

Vogt, BA. Structural organization of cingulate cortex: Areas, neurons, and somatodendritic transmitter receptors. In: Vogt, BA.; Gabriel, M., editors. Neurobiology of Cingulate Cortex and Limbic Thalamus: A Comprehensive Handbook. Birkhäuser; Boston: 1993. p. 19-70.

Vogt BA, et al. Cingulate cortex of the rhesus monkey: I. Cytoarchitecture and thalamic afferents. J Comp Neurol. 1987; 262:256–270. [PubMed: 3624554]

Walsh DM, Selkoe DJ. Deciphering the Molecular Basis of Memory Failure in Alzheimer's Disease. Neuron. 2004; 44:181–193. [PubMed: 15450169]

Wang B, et al. Glutamatergic components of the retrosplenial granular cortex in the rat. Journal of Neurocytology. 2001; 30:427–441. [PubMed: 11951053]

Wong-Riley MT. Cytochrome oxidase: an endogenous metabolic marker for neuronal activity. Trends Neurosci. 1989; 12:94–101. [PubMed: 2469224]

Wyss JM, van Groen T. Connections between the retrosplenial cortex and the hippocampal formation in the rat: A review. Hippocampus. 1992; 2:1–11. [PubMed: 1308170]

Xie S, et al. Voxel-based detection of white matter abnormalities in mild Alzheimer disease. Neurology. 2006; 66:1845–1849. [PubMed: 16801648]

Zhang Y, et al. Diffusion tensor imaging of cingulum fibers in mild cognitive impairment and Alzheimer disease. Neurology. 2007; 68:13–9. [PubMed: 17200485]

Zhou Y, et al. Abnormal connectivity in the posterior cingulate and hippocampus in early Alzheimer's disease and mild cognitive impairment. Alzheimer's and Dementia. 2008; 4:265–270.

Europe PMC Funders Author Manuscripts

Europe PMC Funders Author Manuscripts

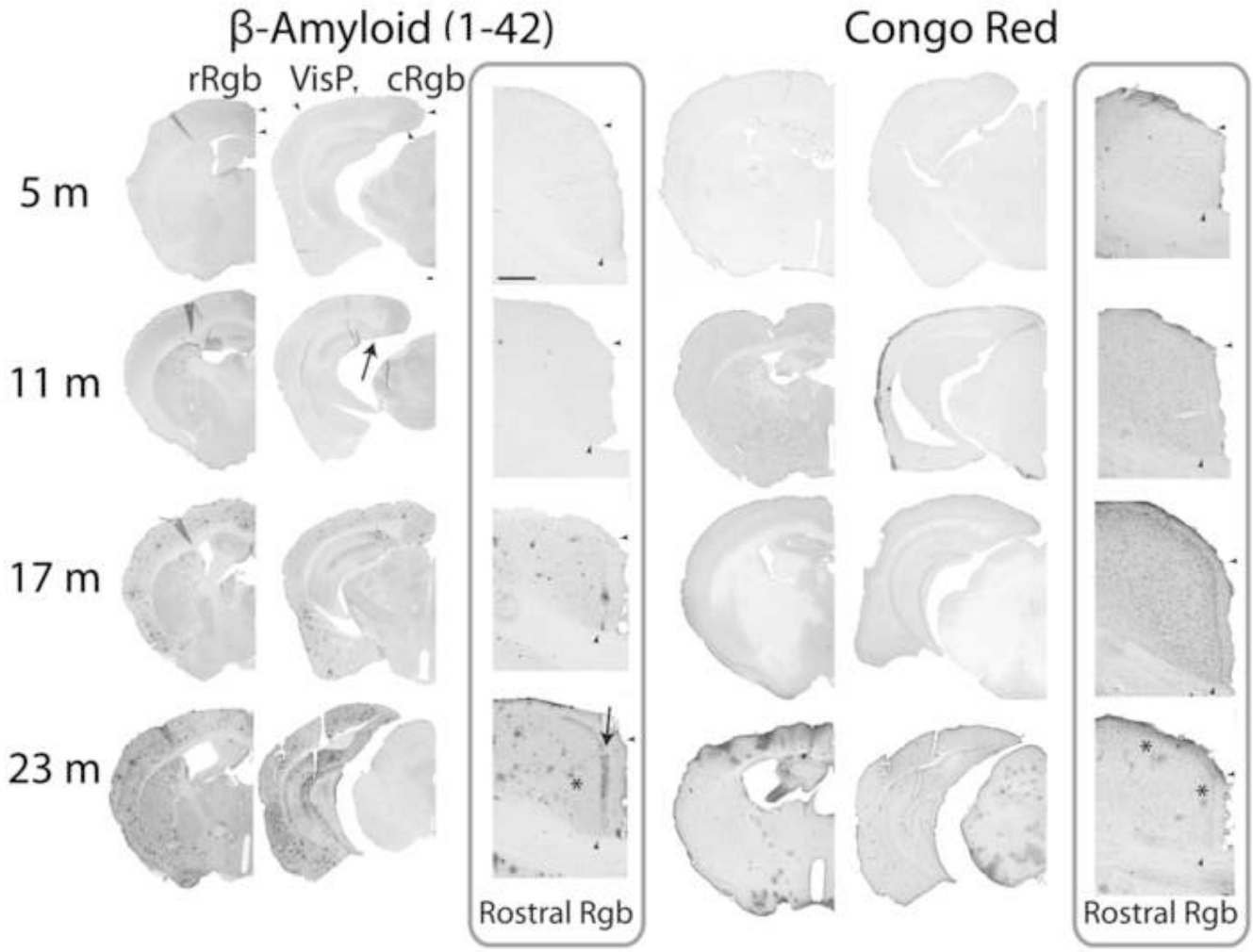

Figure 1. Ageing and amyloid accumulation in Tg2576 mice [β-amyloid $_{(1-42)}$, Congo Red (with Nissl counterstain)].

For each marker, a representative photomontage demonstrates the extent of labeling, while a 5× photomicrograph presents specifically the progression of pathology in the retrosplenial cortex (rostral). Small deposits of β-amyloid $_{(1-42)}$ label can be detected at 11 months sometimes, usually appearing in the subiculum and adjacent forceps major of corpus callosum (arrow). Next, pervasive labeling can be seen at 17 months, including in the retrosplenial cortex, followed with widespread and intense label at 23 months. Notice the distinctive superficial laminar pattern of diffuse extracellular amyloid accumulation seen with increasing age in the retrosplenial cortex (arrow). Congophilic cored plaques appear occasionally in the hippocampal formation at 17 months, extending into the cortex at 23 months, including a few in the retrosplenial cortex (* shows example). Arrowheads indicate the limit of the rostral and caudal granular b retrosplenial cortex (r- and cRgb), including the boundary between superficial and deep laminae, as well as that of the primary visual cortex (VisP). Scale bars = 200 μm.

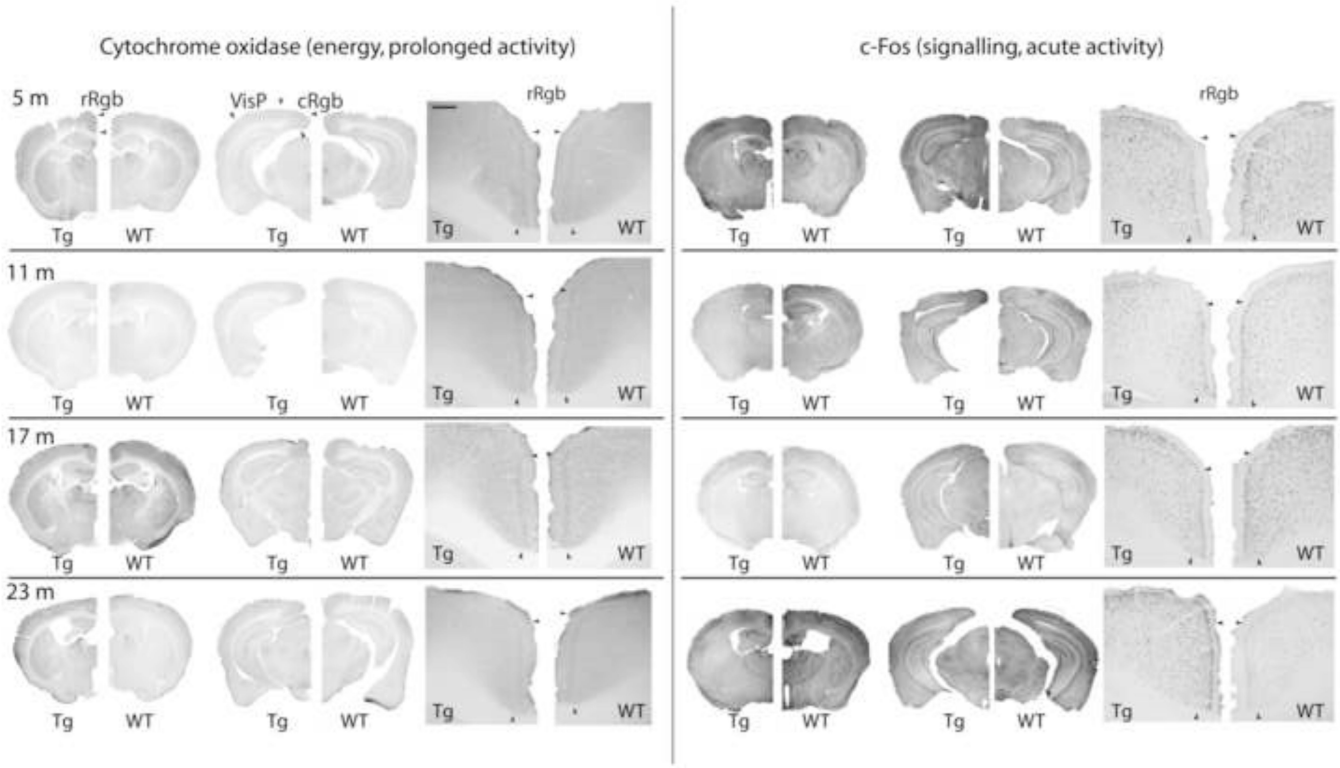

Figure 2. Effect of ageing on activity markers in Tg2576 mice.

Neural reactivity is indicated by c-Fos immediate-early gene induction, and energy metabolism with cytochrome oxidase. For each marker, a representative photomontage demonstrates the pattern of labeling, while a 5× photomicrograph presents specifically the progression of pathology in the retrosplenial cortex (rostral). Note that for the quantification of the intensity of cytochrome oxidase activity, optical densities are normalized to adjacent white matter, while c-Fos cell quantification is based on an intensity threshold from background levels to reduce inherent batch variability. Visual comparisons are done within-age groups, statistical analyses being based on normalized values, as described in the methodology. Arrowheads indicate the limit of the rostral and caudal granular b retrosplenial cortex (r- and cRgb), including the boundary between superficial and deep laminae, as well as that of the primary visual cortex (VisP). Scale bars = 200 μm.

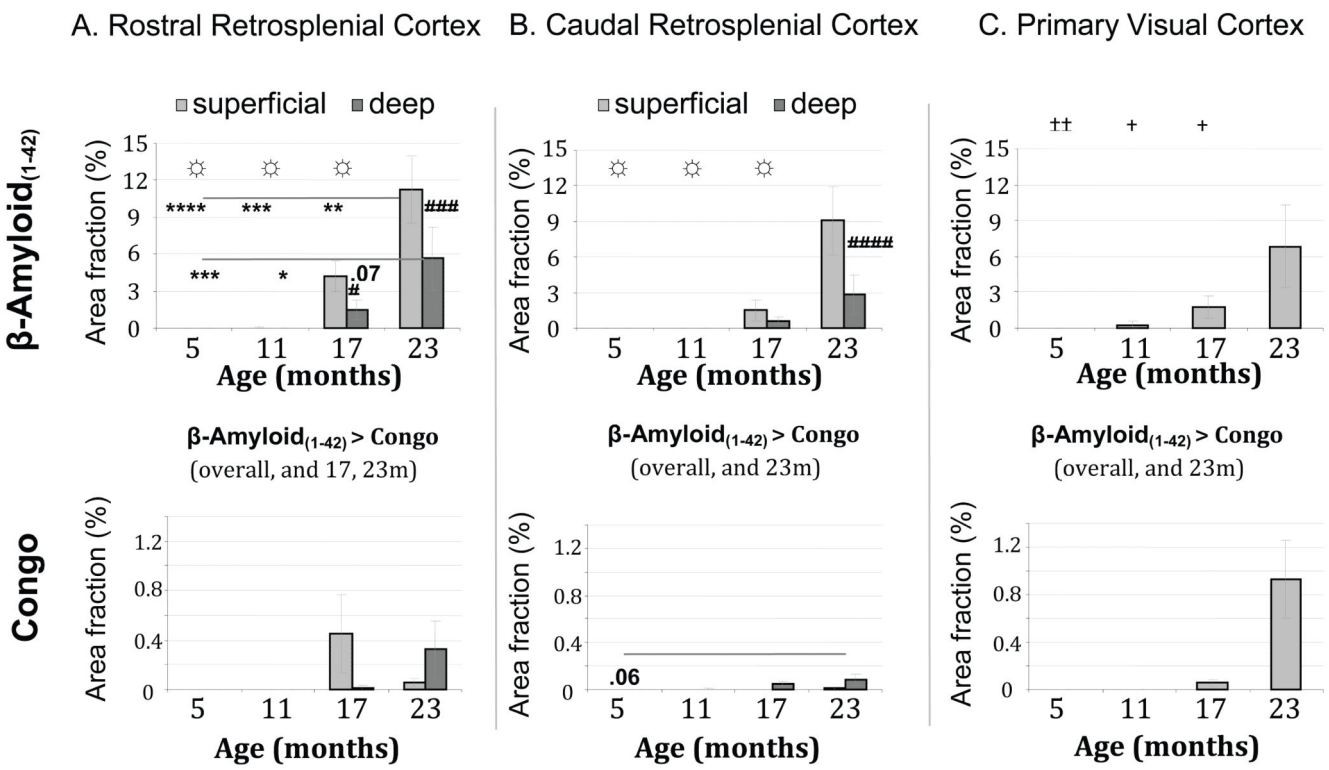

Figure 3. Histograms of amyloid deposition across age groups of transgenic mice.

For rostral retrosplenial (Rgb) cortex, the load of β-Amyloid$_{(1\text{-}42)}$ increased with age (‡, between age groups over both markers; *, across age groups for each laminae per marker, **** $p < 0.001$; *** $p < 0.005$; ** $p < 0.01$; * $p < 0.05$); whereas formation of congophilic material was relatively less abundant (☼, between age groups for single marker). β-Amyloid$_{(1\text{-}42)}$ burden was preferentially found in superficial laminae (#, between superficial and deep laminae within age group). Amyloid also accumulated significantly in the caudal portion of the retrosplenial cortex, but it appeared less pronounced than in the rostral portion. In the primary visual cortex, amyloid load was only significant at 23 months, cored congophilic plaques again less abundant than β-Amyloid$_{(1\text{-}42)}$-labeled material. Errors bars represent the standard error of the mean.

Europe PMC Funders Author Manuscripts

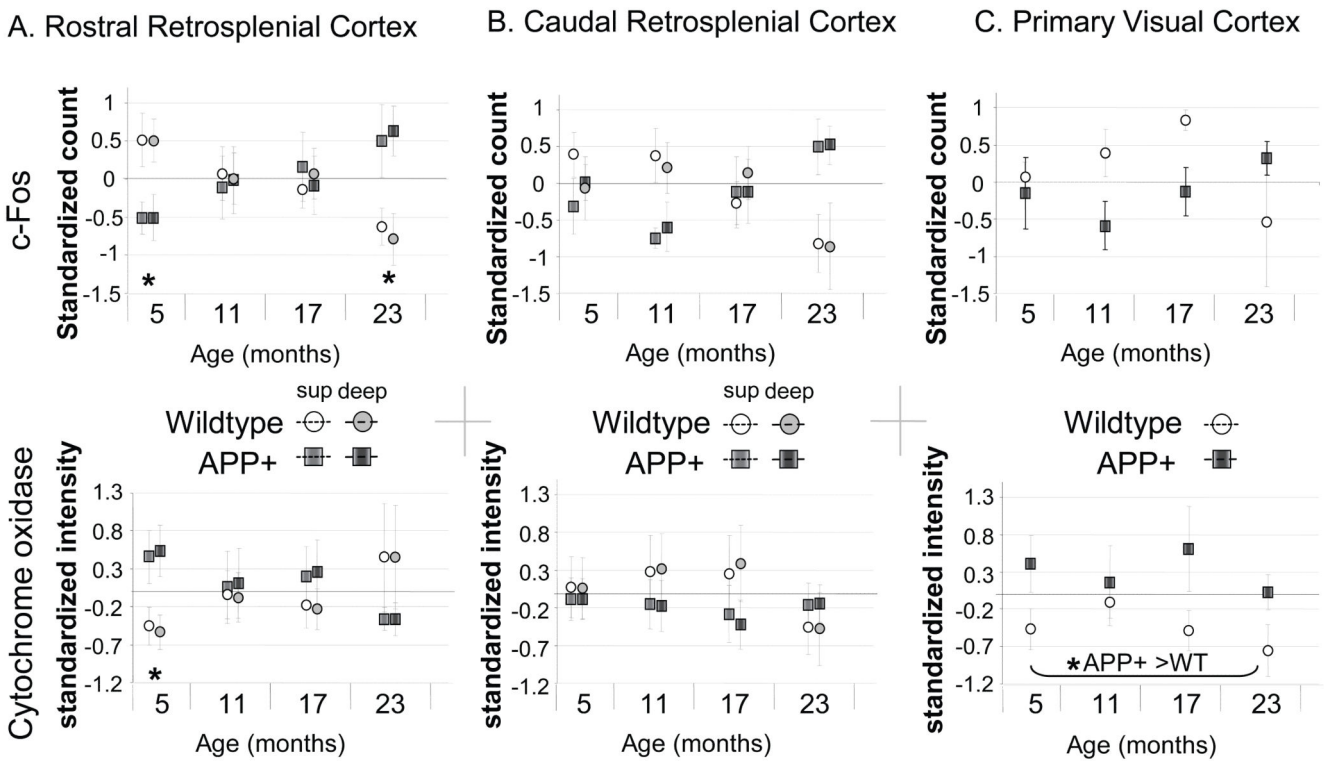

Figure 4. Histograms of cellular activity markers for wildtype and transgenic APP+ mice across age groups.

Cytochrome oxidase and c-Fos were both only altered for rostral Rgb at 5 months (top left panel). In addition to being reduced at 5 months, c-Fos induction was greater than wildtype mice at 23 months. The primary visual cortex exhibited chronic hypermetabolism. Errors bars represent the standard error of the mean. * $p < 0.05$.

Europe PMC Funders Author Manuscripts

Europe PMC Funders Author Manuscripts

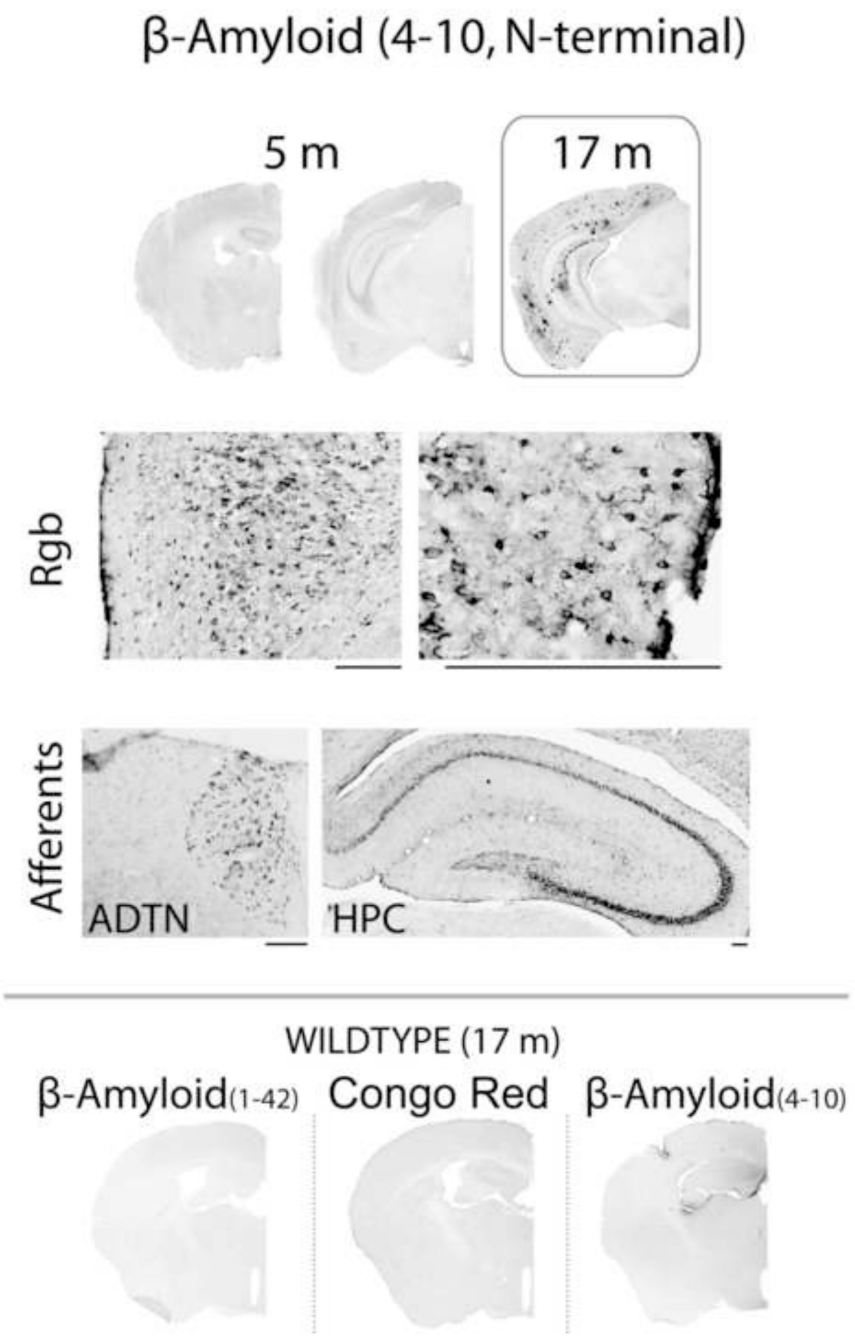

Figure 5. β-amyloid $_{(4-10)}$ pathology in 5-month old APP+ mice.

Marked β-amyloid $_{(4-10)}$ label was observed in the retrosplenial cortex and some of its afferents (top panel, right and inset), months before the appearance of Congo-positive plaques and of material labeled with β-amyloid$_{(1-42)}$ (Fig. 2). The distribution of amyloid accumulation appears to be selectively associated with cells. In contrast, at 17 months the appearance of β-amyloid $_{(4-10)}$ appears equivalent to that of β-amyloid $_{(1-42)}$. Rgb, retrosplenial cortex granular b area; ADTN, anterodorsal thalamic nucleus; HPC, hippocampus. Scale bar = 200 μm.

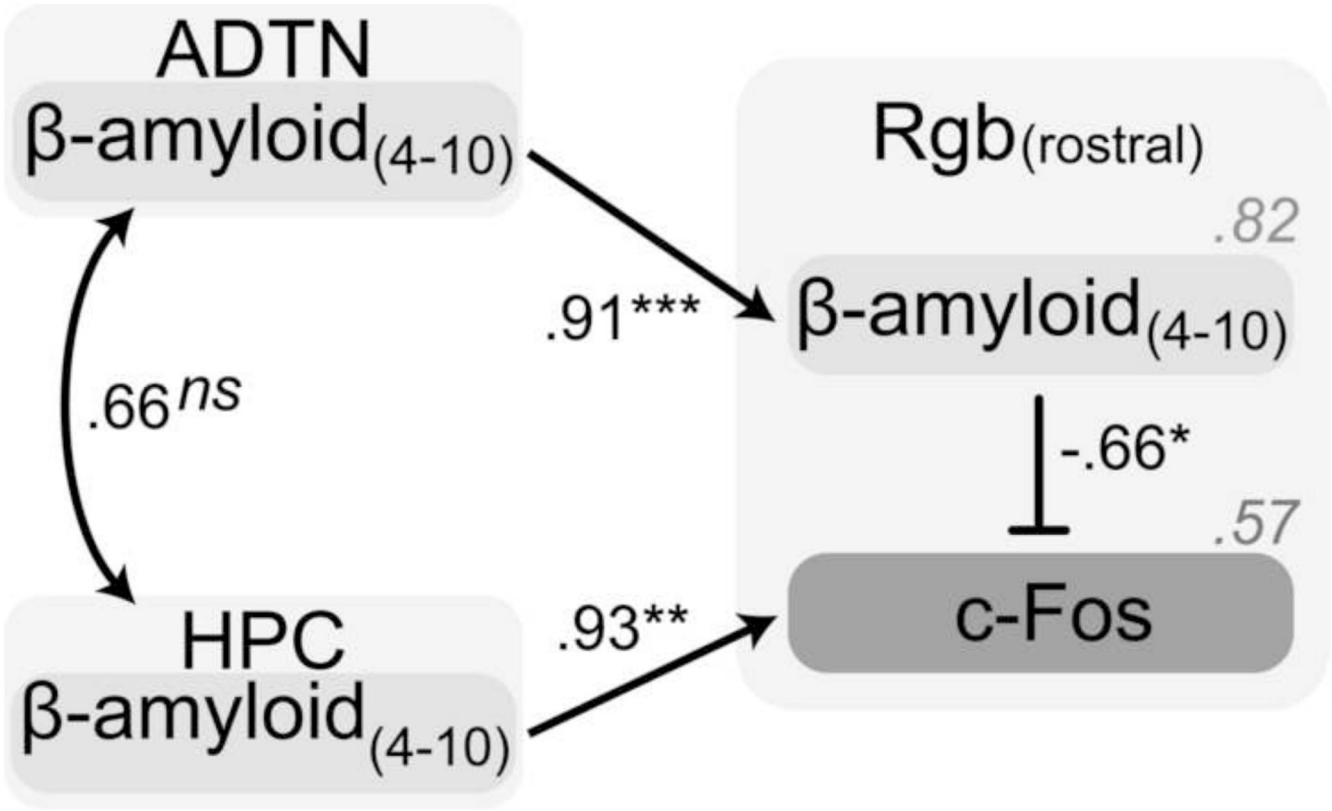

Figure 6. Statistical path analyses for the evaluation of the influence of intrinsic and extrinsic sources of early APP(swe)-related pathology [W0-2, β-amyloid$_{(4-10)}$] on retrosplenial cortex dysfunction (c-Fos) at 5 months.

Anterior thalamus W0-2 seems related to that found in the retrosplenial cortex, which in turn affects c-Fos induction. In contrast, rostral hippocampal W0-2 itself is only a good predictor of retrosplenial cortex c-Fos activity. The blunt arrow represents inhibition while normal arrows represent increase/activation. Italicized values represent the coefficient of determination, a value representing the amount of variance accounted for by the explanatory variables. ADTN, anterior thalamic nuclei; HPC, hippocampus; Rgb, retrosplenial granular b. *, $p < 0.05$; **, $p < 0.005$; ***, $p < 0.001$; *ns*, non-significant ($p > 0.12$).

Europe PMC Funders Author Manuscripts

Europe PMC Funders Author Manuscripts

Table 1

Numbers of subjects per histological analysis.

		Subjects								
			Wild Type				Transgenic			
		Age	5	11	17	23	5	11	17	23
		Region								
Marker	Amylloid burden	rRSC					9/9	6/6	7/8	5/5
		cRSC					9/9	6/6	8/8	5/5
		VisP					9/9	6/6	8/8	5/5
	Cellular activity	rRSC	9/9	9/9	9/9	4/4	9/9	6/6	8/8	5/5
		cRSC	9/9	9/9	6	3/4	9/9	5/6	6/8	5/5
		VisP	7/9	9/9	5/9	3/4	8/9	6/6	4/8	5/5

Table 2

Descriptive data for the area measure of each region according to genotype and age.

Area	*Age (months)*	*WT*			*Tg*		
		N	**Mean (μm²)**	**S.E.M.**	**N**	**Mean (μm²)**	**S.E.M.**
Rostral Rgb (superficial laminae)	5	9	52755.5	4800.7	9	64485.3	7206.6
	11	9	42989.0	2045.3	6	40981.8	3025.0
	17	7	46775.8	2944.4	8	50948.2	2182.1
	23	4	45408.4	4088.8	5	47963.0	5835.2
Rostral Rgb (deep laminae)	5	9	168029.8	11537.3	9	154420.2	11993.6
	11	9	154671.1	7808.3	6	146440.8	11352.9
	17	7	178099.7	13905.1	8	165688.0	8247.6.0
	23	4	161061.6	23249.0	5	155884.0	16763.8
Caudal Rgb (superficial laminae)	5	7	83890.6	6126.7	9	101086.8	5987.8
	11	9	98591.9	6904.5	5	109883.9	13305.0
	17	6	96162.7	8232.4	7	96260.4	6160.6
	23	4	85462.7	7169.3	5	100649.2	7453.5
Caudal Rgb (deep laminae)	5	7	361608.7	31816.9	9	398202.4	29807.8
	11	9	380277.3	18323.0	5	383971.7	33223.6
	17	6	382019.5	16359.8	7	402355.4	27476.9
	23	4	312330.4	25507.5	5	349527.9	12124.6
Primary visual cortex	5	6	853252.0	57186.8	9	931291.6	31945.2
	11	9	917839.2	40754.0	6	841649.1	88381.2
	17	6	778514.6	26882.2	5	760598.9	41592.9
	23	4	692076.4	72379.4	5	840389.9	27825.1